Dissociative Photoionization Mechanism of 1,8-Dihydroxyanthraquinone: An Experimental and Theoretical Study

Yang Pan, Lidong Zhang, Huijun Guo, and Fei Qi*

National Synchrotron Radiation Laboratory, University of Science and Technology of China, Hefei, Anhui 230029, P. R. China

Received: July 13, 2008; Revised Manuscript Received: August 28, 2008

The photoionization and dissociative photoionization mechanism of 1,8-dihydroxyanthraquinone (1,8-DHAQ) have been investigated by infrared laser desorption/tunable synchrotron vacuum ultraviolet photoionization mass spectrometry (IR LD/VUV PIMS) technique and theoretical calculations. Consecutive losses of two carbon monoxides and elimination of hydroxyl group are found to be the major fragmentation channels in low photon energy range. Photoionization efficiency (PIE) spectrum of 1,8-DHAQ was measured in the photon energy range of 8.2−15.0 eV. Adiabatic ionization energy (IE) of 1,8-DAHQ (M) and appearance energies (AEs) of the major fragments $(M-CO)^+$, $(M-C_2O_2)^+$, and $(M-OH)^+$ are determined to be 8.54 ± 0.05, 10.8 ± 0.1, 11.0 ± 0.1, and 13.1 ± 0.1 eV, respectively, which are in fair agreement with calculated results. The B3LYP method with the 6-31+G(d) basis set was used to study fragmentation of 1,8-DHAQ. Theoretical calculations indicate that five lowest-energy isomers of 1,8-DHAQ cations can coexist by virtue of bond rotation and intramolecular proton transfer. A number of decarbonylation and dehydroxylation processes of 1,8-DHAQ cations are well established.

1. Introduction

1,8-Dihydroxyanthraquinone is a component of laxatives and Chinese herbal medicines, such as senna (*Cassia senna*) and aloe, and is known to be a potential mutagen or carcinogen.[1] In addition, it is also a constituent of the chromophore of hypericin, a polycyclic quinone which naturally exists in St. John's wort (*Hypericum perforatum L.*) and other plants of the Hypericum genus. Hypericin can act as a photosensitizer in photodynamical therapy of cancer.[2,3] Recently, it was found that 1,8-DHAQ can attenuate β-amyloid-induced neurotoxicity in murine cortical culture system.[4]

Hydrogen bond is one of the weak chemical interactions, and it plays crucial roles in a lot of chemical and biochemical processes. Intramolecular hydrogen bond can influence molecular stability and induce tautomerization via a proton transfer (PT). Ferreiro et al. demonstrated that 1,8-DHAQ in its most stable ground state exhibits two intramolecular hydrogen bonds (O−H···O).[5] Calculations with different basis sets indicate that the presence of hydrogen bonds in neutral 1,8-DHAQ does not favor the exchange of proton.[5] Thus, only one structure can exist in gas phase. Upon irradiation, photoinduced excited-state intramolecular PT process of 1,8-DHAQ will take place, which has been widely studied[3,6−10] to understand its role as intramolecular hydrogen-bonded chromophores in anthracycline antitumor antibiotics.[11−13] Steady fluorescence spectroscopy of 1,8-DHAQ is characterized by a prominent double fluorescence emission, where the shorter wavelength emission is originated from the locally excited (LE) state, and the red-shifted longer wavelength emission is originated from the product of the PT.[14,15] The relative populations of LE and PT states depend on the polarity of solvent. Time-resolved fluorescence spectra of 1,8-DHAQ reveal that both the normal-form-type fluorescence and the tautomeric-form-type fluorescence appear almost instantaneously, which suggests that a barrierless excited-state PT occurs within 50 fs, reflecting delocalization of the excited-state wave function.[6] In addition, a spectral change was also found in time scale of a few picoseconds. In another time-resolved experiment, the fluorescence excitation spectrum of 1,8-DHAQ exhibits two obvious excess energy ranges, which are characterized by different spectral congestions and relative intensities in the frequency-domain measurements and by different fluorescence lifetimes in the time-domain measurements.[3] Time-resolved excited state (S_1) absorption and stimulated emission experiments showed that the electronic excitation of 1,8-DHAQ yields a diffused excited state, essentially delocalized over the very broad S_1 state, which extends to both tautomeric species.[9] All these measurements testify the importance of excited-state intramolecular PT process which occurs with 1,8-DHAQ.

As hydroxyl-substituted anthraquinones, elementary fragmentation channels of 1-hydroxyanthraquinone (1-HAQ), 2-hydroxyanthraquinone (2-HAQ), 1,2-dihydroxyanthraquinone (1,2-DHAQ), 1,5-dihydroxyanthraquinone (1,5-DHAQ), 1,8-DHAQ, and so forth, were studied with electron-impact ionization mass spectrometry (EI-MS).[16,17] In these cases, the losses of hydroxyl group and neutral carbon monoxides were found to be the dominant decomposition pathways. However, because of the influence of hydrogen bond and subsequent intramolecular PT processes, fragmentation pathways of these hydroxyanthraquinones are far more complex than we have known. For example, the elimination of carbon monoxide can occur with carbonyl group or C−O(H) group of hydroxyanthraquinones. Proctor et al. have labeled the carbonyl oxygens with ^{18}O without enrichment of the hydroxyl oxygen of 1-HAQ and distinguished the relative probabilities of $(M-CO)^+$ ion formed from these two groups.[17] Moreover, the relative abundance for $(M-OH)^+$ from 1,2-DHAQ was found to be higher than those of the hydroxyl groups on each benzene ring, such as 1,5-DHAQ and 1,8-DHAQ, whereas the relative abundance of $(M-OH)^+$ from

* Corresponding author. E-mail: fqi@ustc.edu.cn. Fax: +86-551-5141078. Tel: +86-551-3602125.

10.1021/jp806171h CCC: $40.75
Published on Web 10/02/2008

2,6-DHAQ is the greatest.[16] It seems that the loss of hydroxyl group is greatly influenced by the presence or absence of intramolecular hydrogen bond. Compared to extensively spectroscopic studies, photoionization mass spectrometric study of 1,8-DHAQ and its fragmentation are scarce. This is partly due to its nonvolatile character that is prerequisite for mass spectrometric analysis.

More recently, we have used IR LD/VUV PIMS to investigate the fragmentation pathways of six quinones including 1,2-naphthoquinone (1,2-NQ), 1,4-naphthoquinone (1,4-NQ), 9,10-phenanthroquinone (PQ), 9,10-anthraquinone (AQ), benz[a]anthracene-7,12-dione (BAD), and 1,2-acenaphthylene-dione (AND) and measured the AEs for the consecutive losses of two carbon monoxides.[18] In this work, we report the photoionization and dissociative photoionization investigation of 1,8-DHAQ performed by using the same technique and ab initio calculations. Ionization energy and appearance energies of major fragments were obtained by measurements of photoionization efficiency spectra. Moreover, to understand the effects of hydrogen bonds/intramolecular PT after photoionization, the interconversion of different parent/fragment isomers and major fragmentation pathways, we carried out a detailed theoretical study by using the B3LYP method. All the energies of isomeric structures resulting from intramolecular PT and intermediates are discussed in detail.

2. Experimental and Theoretical Methods

2.1. Experimental Method. The instrument of IR LD/VUV PIMS has been described elsewhere.[18−20] Therefore, only a short description is given here. 1,8-DHAQ was purchased from Fluka and used without further purification. The sample is coated on a stainless steel substrate without any organic matrix. IR LD/VUV PIMS utilizes 1064 nm output of a pulsed Nd:YAG laser (Surelite I-20, Continuum, USA) at the operation rate of 10 Hz for laser desorption on the substrate. The laser beam is focused to a spot of 0.5−1.0 mm in diameter on the surface of the substrate. Laser power is controlled at about 1.0 mJ/pulse to generate intact neutral molecules for near-threshold VUV photoionization. Tunable VUV light beam from a synchrotron is perpendicular and overlapping with the desorption plume in the photoionization region. VUV photoionization takes place at a distance of ∼2−4 mm from the substrate surface, where the plume of molecules formed from the desorption travel back and are ionized by the VUV light. Ions produced by the VUV light are analyzed by a reflectron time-of-flight mass spectrometer.[21] A pulsed voltage of 260 V with a frequency of 10 kHz applied to the repeller plates is used to extract ions into the flight tube. The acceleration voltage is kept at 2000 V. The mass resolution ($m/\Delta m$) and mass range are measured to be around 1400 and 600 (Da), respectively. Time delay between the Nd:YAG laser and the pulse of the extract field is 150 μs, which is controlled by a homemade pulse/delay generator. The ion signals are detected with microchannel plates (MCP) and then amplified by a preamplifier VT120C (ORTEC, USA). A multiscaler P7888 (FAST Comtec, Germany) records the TOF spectrum with a bin width of 2 ns. A small bias voltage (1.0 V) is used to improve signal intensity, reduce the background ions, and enhance the mass resolution.[22] The pressure of photoionization chamber is around 1.0×10^{-4} Pa.

Synchrotron radiation from an undulator of the 800 MeV electron storage ring of National Synchrotron Radiation Laboratory (NSRL) is monochromatized with a 1 m Seya-Namioka monochromator equipped with a laminar grating (1500 grooves/mm, Horiba Jobin Yvon, France). This grating covers the photon energy from 7.8 to ∼24.0 eV. The monochromator is calibrated with the known ionization energies of the inert gases. The energy resolving power ($E/\Delta E$) is about 1000. A gas filter filled with helium or argon is used to eliminate higher-order radiation. The average photon flux is measured to be around 1×10^{13} photons/s. A silicon photodiode SXUV-100 (International Radiation Detectors, Inc., USA) is used to monitor the photon flux for normalizing ion signals.

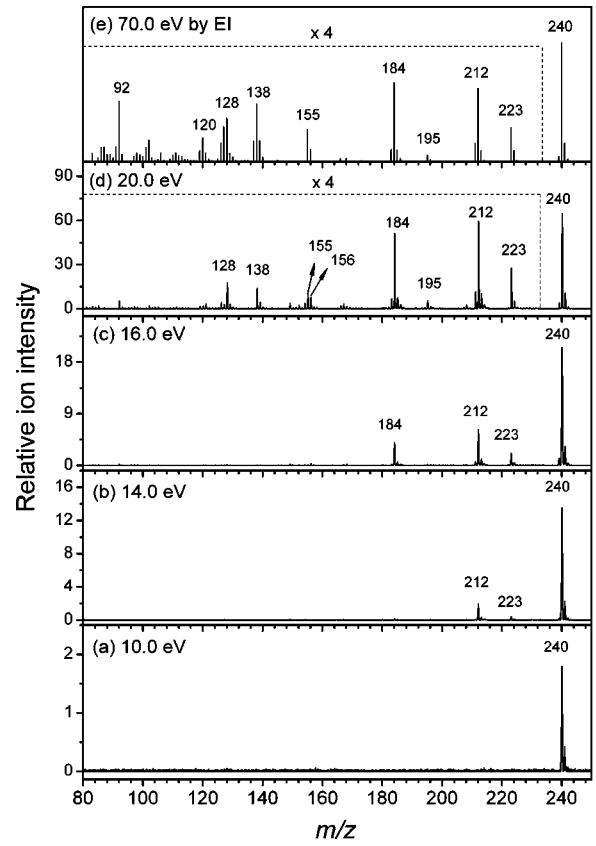

Figure 1. Photoionization mass spectra of 1,8-DHAQ at the photon energies of (a) 10.0 eV, (b) 14.0 eV, (c) 16.0 eV, and (d) 20.0 eV. (e) Mass spectrum of 1,8-DHAQ with 70 eV EI (adapted from NIST webbook).[27]

2.2. Computational Method. Ab initio calculations were carried out by using the Gaussian 03 program.[23] The geometries of 1,8-DHAQ were fully optimized at the hybrid density functional B3LYP/6-31+g(d) level. The vibrational frequencies were calculated at the same level for characterizing the nature of structure, which were also used to compute the zero-point energy (ZPE). The vertical IE value of the highest occupied molecular orbital (HOMO) was calculated at the P3/6-311G(d,p) level according to electron-propagator theory in the partial third-order (P3) approximation.[24] Ortiz et al. have proven that the calculations performed by using the P3 method with 6-311G(d,p) basis set can get more accurate vertical IE values.[25,26]

3. Results and Discussion

3.1. Photoionization Mass Spectra and Photoionization Efficiency Spectra. Figure 1a−d demonstrates the mass spectra of 1,8-DHAQ ionized at the VUV photon energies of 10.0, 14.0, 16.0, and 20.0 eV. At the photon energy of 10.0 eV, only molecular ion peak M^+ at $m/z = 240$ is yielded by virtue of near-threshold soft photoionization. Fragments are gradually produced with excitation photon energy increasing. At a photon energy of 14.0 eV, besides the peak of the molecular ion, a

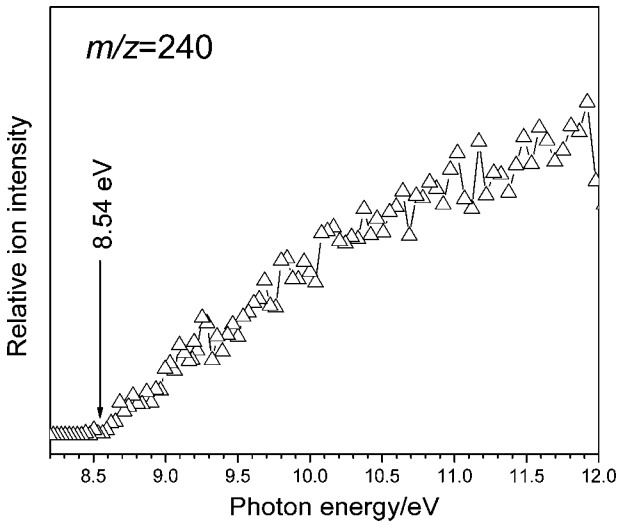

Figure 2. PIE spectrum of 1,8-DHAQ ($m/z = 240$).

peak at $m/z = 212$ accompanied by another relative weak fragment at $m/z = 223$ are also observed, which are attributed to the $(M-CO)^+$ and $(M-OH)^+$ ions, respectively. When the photon energy is increased to 16.0 eV, the elimination of the second carbon monoxide from molecular ion yields the fragment at $m/z = 184$. At the photon energy of 20.0 eV, more fragments are obviously detected at $m/z = 156$, 155, 138, 128, and so forth. The peak at $m/z = 156$ corresponds to the loss of the third CO group. In comparison, another relative weak fragment at $m/z = 155$ is ascribed to the $(M-C_3O_3H)^+$ ion. The fragment at $m/z = 138$ may be due to the loss of H_2O from the $(M-C_3O_3)^+$ ion or loss of OH radical from the $(M-C_3O_3H)^+$ ion. The elimination of the fourth CO group produces the fragment of $(M-C_4O_4)^+$ at $m/z = 128$. Figure 1e shows the mass spectrum with 70.0 eV electron impact ionization,[27] which exhibits similar characteristics to the mass spectrum measured at the photon energy of 20.0 eV.

Photoionization mass spectra of 1,8-DHAQ suggest the preliminary fragmentation pathways below 15.0 eV photon energy are the consecutive losses of two carbon monoxides and an additional elimination of hydroxyl radical. The loss of CO followed by the elimination of OH (or the loss of OH followed by the elimination of CO) is another fragmentation process, which may form the fragment ion at $m/z = 195$. The relative abundance of this fragment, however, is too low (1.3% by 70.0 eV EI and 2.1% by 20.0 eV PI) to be emphasized in this work. Moreover, consecutive losses of two hydroxyl groups are impossible dissociation channels. Thus, only dominant fragments of $(M-CO)^+$, $(M-C_2O_2)^+$, $(M-OH)^+$ and corresponding fragmentation pathways are focused and discussed in this paper.

Ionization energy can be determined by measurement of the PIE spectrum, which is obtained by plotting the integrated mass peak versus corresponding photon energy. The PIE spectrum of 1,8-DHAQ cation is obtained at the photon-energy range from 8.2 to 12.0 eV, as shown in Figure 2. The onset in the PIE spectrum appears clearly and is definitely determined to be 8.54 $\pm$ 0.05 eV, which corresponds to the IE of 1,8-DHAQ. The PIE spectra of the fragment ions $(M-OH)^+$, $(M-CO)^+$, and $(M-C_2O_2)^+$ at $m/z = 223$, 212, and 184 are shown in Figure 3a,b,c, respectively. As can be seen clearly, these PIE spectra exhibit gradual onsets and extend toward lower photon energies. Such ambiguous feature makes it difficult to judge the relative accurate onsets. Some attempts have been made to explain the tail or step-like character in PIE spectra of molecules and

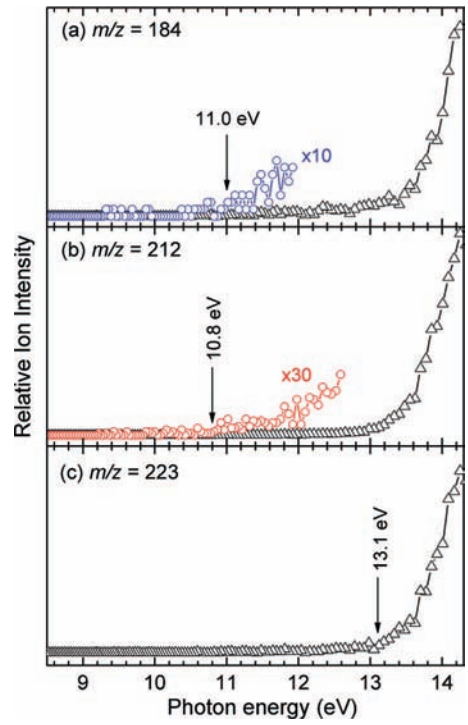

Figure 3. PIE spectra of the fragments at (a) $m/z = 184$, (b) $m/z = 212$, and (c) $m/z = 223$.

TABLE 1: IE and AEs for the parent and fragments of 1,8-DHAQ

			IE/AEs (eV)	
quinone	ions	m/z	this Work	DFT
1,8-DHAQ	M^{+a}	240	8.54 $\pm$ 0.05 eV	8.24
	$(M-OH)^+$	223	13.1 $\pm$ 0.1 eV	13.29
	$(M-CO)^+$	212	10.8 $\pm$ 0.1 eV	10.78
	$(M-C_2O_2)^+$	184	11.0 $\pm$ 0.1 eV	11.17

[a] M^+ denotes parent ion.

clusters.[28-31] Here, the observed tails in our PIE spectra are due to coexistence of several isomeric structures of the cations via intramolecular PT and OH group rotation about the C–O bond. Furthermore, residual internal energy (rotational tailing) may also give rise to such experimental feature. AE of $(M-OH)^+$ ion is determined to be 13.1 $\pm$ 0.1 eV by the intersection of two fitted lines. In the cases of $(M-CO)^+$ and $(M-C_2O_2)^+$ ions, to clearly identify the onsets, parts of the PIE spectra are magnified 10 and 30 times, respectively. AEs of $(M-CO)^+$ and $(M-C_2O_2)^+$ are estimated to be 10.8 $\pm$ 0.1 and 11.0 $\pm$ 0.1 eV, respectively, as summarized in Table 1.

3.2. Calculated Geometries, Ionization Energy, and Appearance Energies. Ferreiro et al. have studied the neutral structure of 1,8-DHAQ with Hartree–Fock method, and only a single minimum with two hydrogen bonds has been identified.[5] Our B3LYP calculations give rise to the same structure, as shown in Figure 4. Here, relative energy of the neutral 1,8-DHAQ is defined to be zero, and the energies of all the other species in this paper are relative to that of 1,8-DHAQ. The lowest-energy structures for five isomeric 1,8-DHAQ radical cations upon ionization are obtained, as shown in Figure 4. Bond distances of these structures are given in angstroms. Optimized cation **1** shows a structure similar to that of the neutral with minor configuration change. The cation **1** is at the global minimum for all cations on the potential energy surface (PES), followed by **2**, **3**, and **4**, which are isomeric products of **1** via

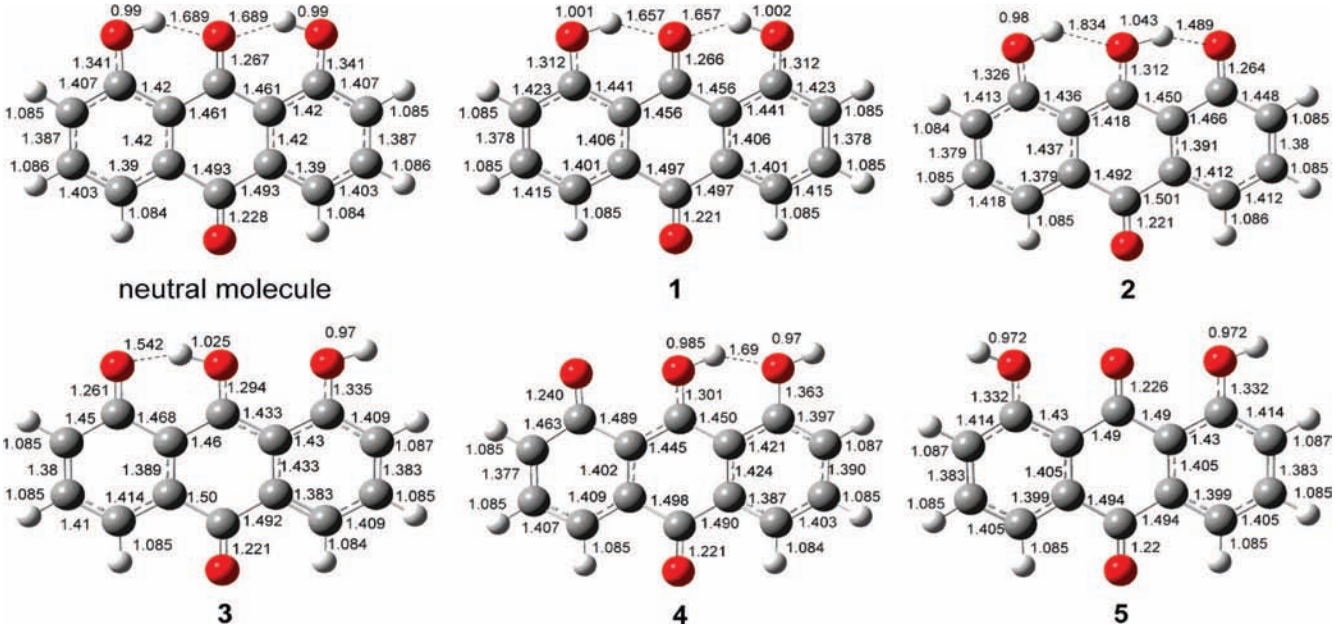

Figure 4. Optimized lowest-energy structures for neutral 1,8-DHAQ and isomeric cations **1**-**5** (bond lengths in Å).

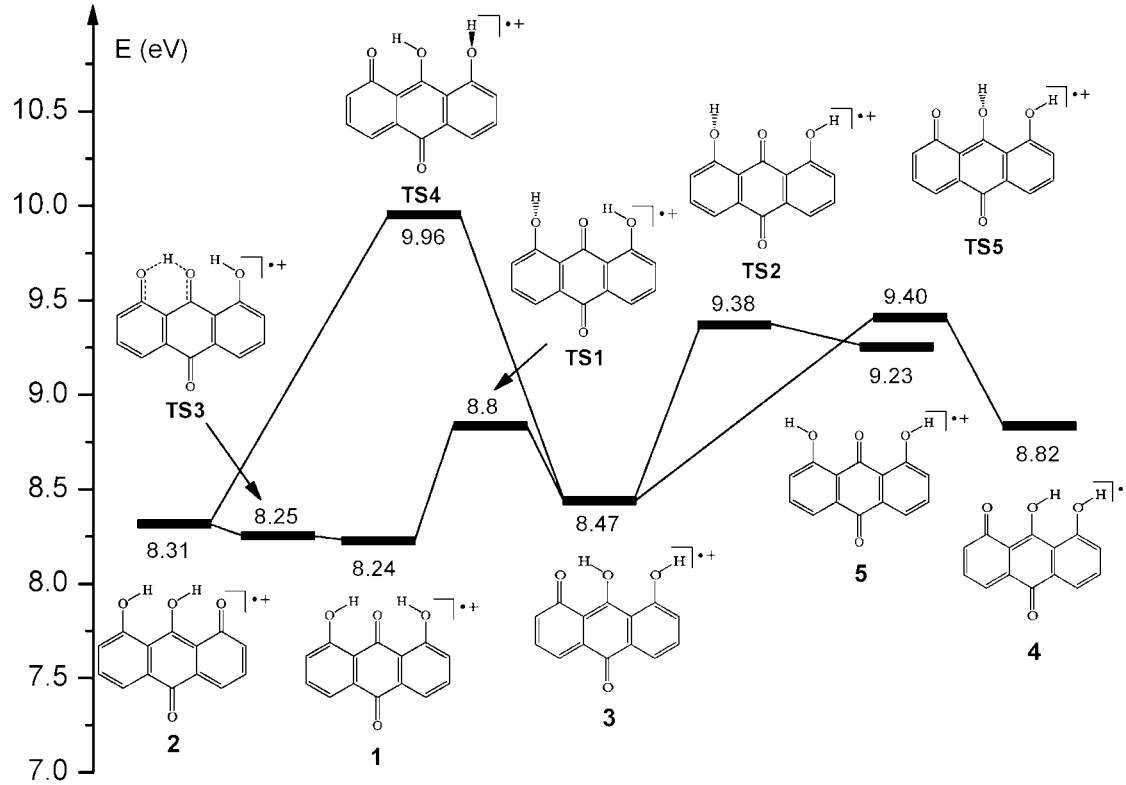

Figure 5. Energy profiles for interconversion between five isomeric 1,8-DHAQ cations. All the energies (in eV) are relative to that of neutral 1,8-DHAQ.

intramolecular PT and C−O bond rotation. Relative stability of each isomer may be related to the degree of delocalization of π cloud over three benzene rings, which is controlled by intramolecular hydrogen bonds.[5] The cation **5** is the highest in energy for all minima on PES. Owing to the lack of hydrogen bonds, this cation is destabilized by 0.99 eV in energy relative to **1**. Figure 5 shows the energy profile for the interconversion of five isomeric cations of 1,8-DHAQ. Energies of the optimized structures and transition states evaluated at the B3LYP/6-31+d(p) level are presented in Table S1 of the Supporting Information. The energies in Table SI are given in hartree relative to that of the neutral structure of 1,8-DHAQ.

The adiabatic ionization energy is considered only for 1,8-DHAQ ionized to the most stable cation **1**. Theoretical calculations give rise to the adiabatic IE value of 8.24 eV, which is slightly lower than the experimental result (8.54 eV). The HOMO of **1** is a delocalized π MO on either side benzene rings, and the vertical IE is calculated to be 8.836 eV at the P3/6-311G(d,p) level. AEs for the losses of carbon monoxides and hydroxyl group are also calculated with the B3LYP method. It is found that consecutive decarbonylation processes could occur on C1, C8, C9, and C10 positions from five isomeric cations via a series of complex transition states and transient intermediates as discussed below. The lowest barriers for the elimination

SCHEME 1: Proposed Decarbonylation Pathways for Five Isomeric 1,8-DHAQ Cations[a]

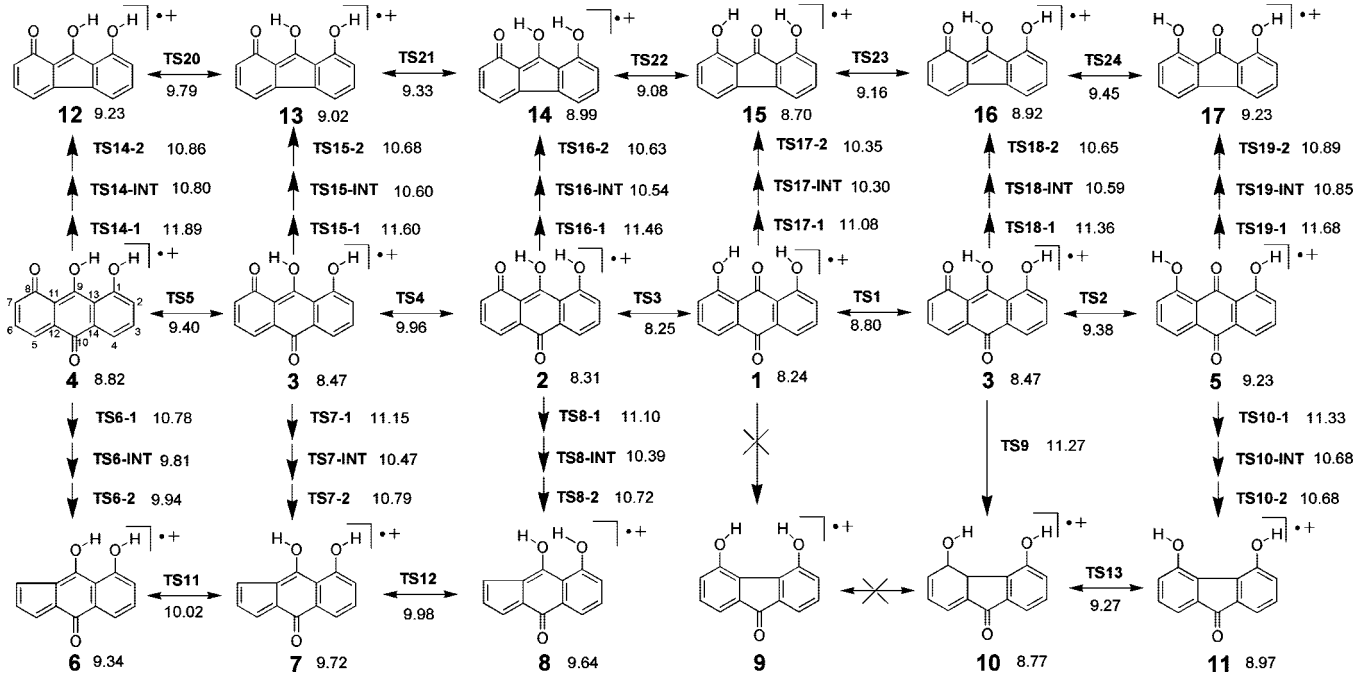

[a] The cross symbol denotes impossible pathway. The relative energies of all species are also labeled (in eV).

SCHEME 2: Proposed Pathways for the Loss of the Second Carbon Monoxide from 11 Isomeric $(M-CO)^+$ Ions[a]

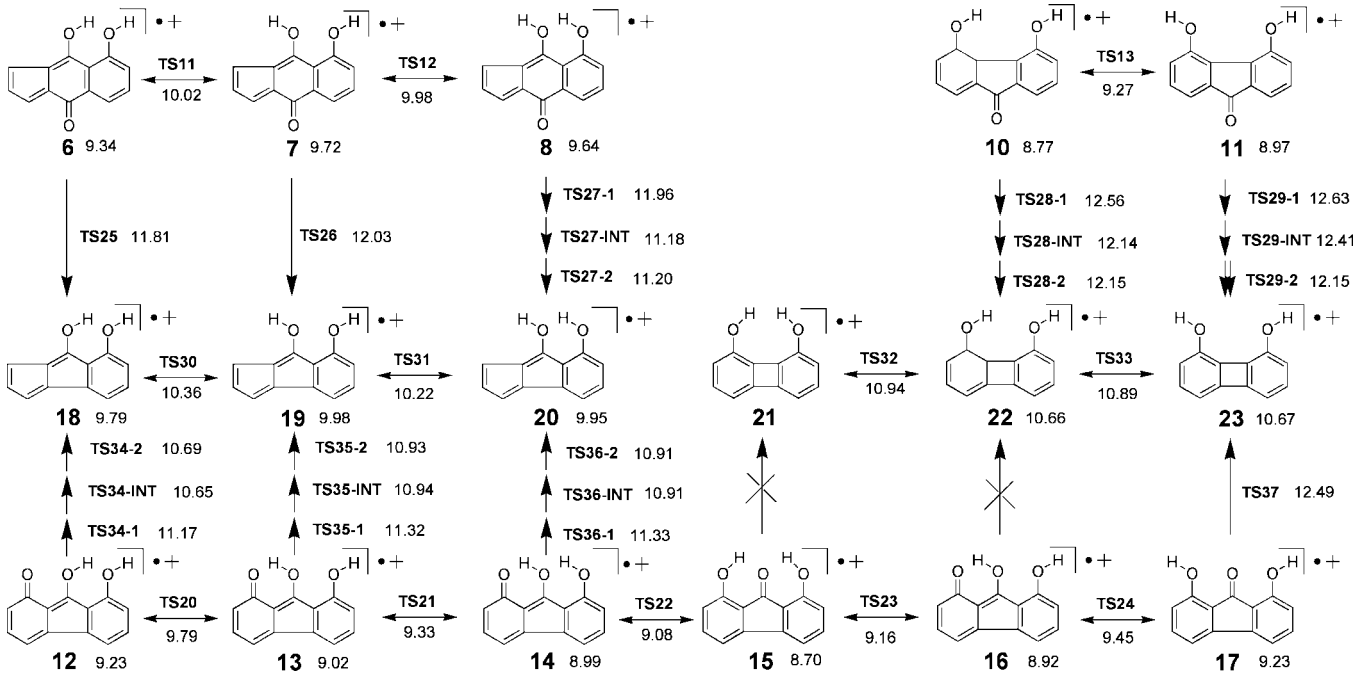

[a] The cross symbol denotes impossible pathway. The relative energies of all species are also labeled (in eV).

of the first and the second carbon monoxide groups are identified to the processes of **4**→**6** and **12**→**18**, as shown in Schemes 1 and 2. Accordingly, theoretical AEs of $(M-CO)^+$ and $(M-C_2O_2)^+$ are determined to be 10.78 and 11.17 eV, respectively, which agree very well with the values of 10.8 ± 0.1 and 11.0 ± 0.1 eV measured from the PIE spectra. Direct dehydroxylation from 1,8-DHAQ cations forms the $(M-OH)^+$ ion. The B3LYP calculations indicate that only loss of OH group after C−O bond (may be C1, C8, or C9) cleavage is favored without undergoing any transition states and intermediates. Processes **1**→**24**, **2**→**24**, and **3**→**24** are found to be most reliable pathways to form the product **24** with the least energy of 13.29 eV, as shown in Scheme 3. Our experimental onset of 13.1 ± 0.1 eV is also in fair agreement with this calculated AE value.

3.3. Elimination of the First Carbon Monoxide Group. All the equilibrium structures along with bond distances for cations, transition states, and intermediates are shown in Figure S1 of the Supporting Information. The calculated B3LYP energies *E* (with ZPE, in hartree), enthalpies *H* (in hartree), and free energies *G* (in hartree) of all the species are also summarized in Table S1 of the Supporting Information. Scheme 1 shows the pathways for the loss of the first CO from five isomeric 1,8-DHAQ cations and their interconversion. A total of 11 potential decarbonylation processes for the molecular ions

SCHEME 3: Proposed Dehydroxylation Pathways for Five Isomeric Cations of 1,8-DHAQ[a]

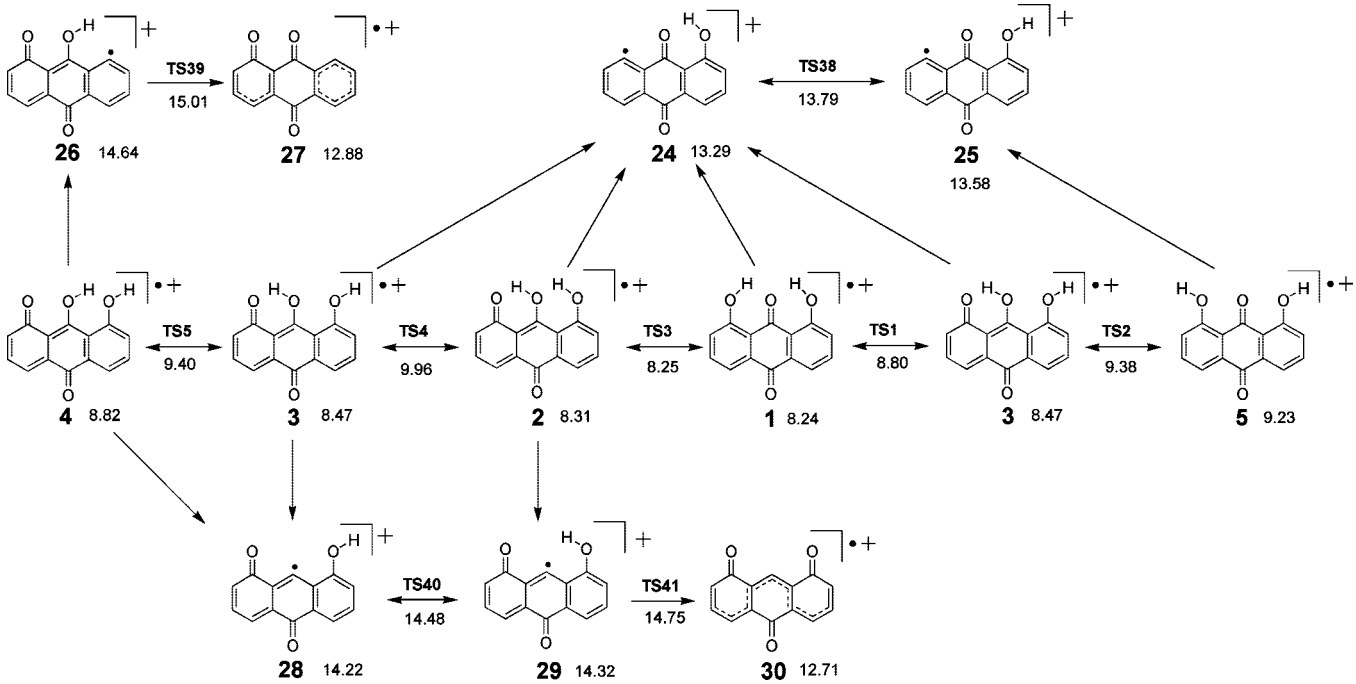

[a] The relative energies of all species are also labeled (in eV).

are found from theoretical calculations. Among these processes, the loss of CO (C8) from the cation **4** occurs with the least energy. The B3LYP results suggest that **4** can undergo C8−C11 bond fission via **TS6−1** to form intermediate **TS6-INT**. Subsequently, **TS6-INT** overcomes a barrier of **TS6−2** to lose CO and yields the product **6**. The barriers for these two steps are 1.96 and 0.13 eV, respectively. Another alternative decarbonylation pathway for **4** first occurs with the C10−C14 bond cleavage to give **TS14-INT**. This step has a relative higher barrier of 3.07 eV. After overcoming a barrier of 0.06 eV at **TS14−2**, the product **12** is formed.

Starting from the cation **3**, four possible fragmentation pathways of decarbonylation are obtained. First, after intramolecular PT from **1**, C8−C11 bond cleavage of **3** via transition state **TS7−1** leads to the formation of intermediate **TS7-INT**. The calculated barrier is 2.68 eV. Then, the C7−C8 bond elongates and breaks with the formation of $(M-CO)^+$ and CO via **TS7−2** with an energy of 0.32 eV. Second, **3** undergoes C10−C14 bond fission with an activation barrier of 3.13 eV at **TS15−1**, generating an intermediate **TS15-INT**. The C10−C12 bond in this intermediate then breaks with an energy of 0.08 eV to produce the product ion **13**. Third, the decarbonylation channel from **3** to the product **10** proceeds via an intramolecular PT and subsequent loss of CO group. The barrier of this step is calculated to be 2.8 eV. Finally, after C10−C12 bond cleavage, intermediate **TS18-INT** is formed via transition state **TS18−1.** C10−C14 bond of **TS18-INT** then breaks and forms the product **16**. The barriers for these two steps are calculated to be 2.89 and 0.06 eV, respectively.

Starting from the cation **2**, two decarbonylation pathways are proposed. As shown in Scheme 1, one is to process as **2→TS8−1→TS8-INT→TS8−2→8**. In this pathway, once intermediate **TS8-INT** is produced, it undergoes elongation of C1−C2 bond to produce **8**. The barriers at **TS8−1** and **TS8−2** are 2.79 and 0.33 eV, respectively. Another pathway is proposed to be **2→TS16−1→TS16-INT→ TS16−2→14**. Energies for the transition states are 3.15 and 0.09 eV, respectively. As to the cation **1**, loss of CO (C9) to form the product **9** is precluded because of the tight O−H···O···H−O effect. The only favored decarbonylation pathway occurs with the fission of C10−C14 bond to form **TS17-INT** via **TS17−1**, followed by overcoming another barrier to yield the product **15**. The barriers for the two processes are 2.84 and 0.05 eV, respectively.

To make the decarbonylation picture complete, we also investigate the cation **5** with a relative higher energy. Because of the lack of intramolecular PT, the loss of CO takes place from C9 or C10 position without any interference from hydroxyl groups on C1 or C8 positions. They are depicted as **5→TS10−1→TS10-INT→TS10−2→11** and **5→TS19−1→TS19-INT→TS19−2→17** (see Scheme 1). Owing to the stereohindrance effect, elimination of CO from C9 or C10 position requires different energies, which are determined to be 2.1 eV at **TS10−1** and 2.45 eV at **TS19−1**, respectively. It is worth noting that some fragment isomers formed from decarbonylation may transform via PT, as demonstrated in Scheme 1. Relative barriers of these transition states are tabulated in Table S1 in the Supporting Information.

The required energy barriers for the formation of $(M-CO)^+$ and carbon monoxide from the cations **1−5** are different, where the least energy is deemed to be the theoretical AE value. Among these fragmentation channels, **TS6−1** produced from the cation **4** is found to have the least energy of 10.78 eV (relative to neutral 1,8-DHAQ), which is selected as AE of $(M-CO)^+$ ion. This value is comparable with experimental value of 10.8 ± 0.1 eV. Energies of other transition states are somewhat higher than that of **TS6−1**, which may contribute to the gradual increase of intensity above onset in the PIE spectrum.

3.4. Elimination of the Second Carbon Monoxide Group. The elimination of the second carbon monoxide are considered with 11 isomeric $(M-CO)^+$ ions, as displayed in Scheme 2. Five relative stable fragments at $m/z = 184$, labeled as **18**, **19**, **20**, **22**, and **23**, are finally formed from the second decarbonylation.

To form the product ion **18**, two channels are obtained from the B3LYP calculations. First, C−C bond fission of **6** and

subsequent loss of CO can form the product **18** via **TS25**. The barrier for this channel is 2.47 eV. Second, a series of processes are described as **12→TS34−1→TS34-INT →TS34−2→18**. The barrier energies for two transition states are 1.94 and 0.04 eV, respectively. Similarly, the cation **7** can undergo the loss of CO (C10) to produce **19** via only one transition state **TS26** with the energy of 2.31 eV. An alternative pathway to form the product **19** from the cation **13** is depicted as **13→TS35−1→TS35-INT →TS35−2→19**. In this pathway, the dominant barrier at **TS35−1** is calculated to be 2.3 eV.

The product ion **20** in Scheme 2 has two formation pathways, which are depicted as **8→TS27−1→TS27-INT→TS27−2→20** and **14→TS36−1→TS36-INT→TS36−2→20**. In the former decarbonylation pathway, the barriers at **TS27−1** and **TS27−2** are 2.32 and 0.02 eV, respectively, whereas in the latter one, two barriers also need to be overcome. The highest energy at of **TS36−1** is determined to be 2.34 eV.

The cation **10** can occur with the C10−C12 bond cleavage to give **TS28-INT**. This step has a barrier of 3.79 eV. After overcoming another barrier of 0.01 eV at **TS28−2**, the product **22** is formed by the fission of C10−C14 bond. The product **22** could also be formed from **23** via OH group rotation about C−O bond. However, direct loss of CO from **16** is not realized according to the B3LYP calculations. C−O bond rotation of **22** may produce **21** with a barrier of 0.28 eV at **TS32**. Direct loss of CO from **15** to produce **21** is also precluded from theoretical calculations.

In the case of the product **23**, two more decarbonylation processes are depicted as **11→TS29−1→TS29-INT→TS29−2→23** and **17→TS37→23**. Starting from the cation **11**, two barriers at **TS29−1** and **TS29−2** are found, respectively. Starting from the cation **17**, only one barrier at **TS37** is found from the B3LYP calculations, which is determined to be 3.26 eV. Scheme 2 also shows the interconversion of six isomeric $(M-C_2O_2)^+$ cations; barriers between them are listed in Table S1 in the Supporting Information. In a word, the calculated lowest AE value of $(M-C_2O_2)^+$ ion is determined to be 11.17 eV with the transition state **TS34−1** (**12→TS34−1**), which is consistent with our experimental measurement (11.0 ± 0.1 eV).

3.5. Elimination of Hydroxyl Group. Formation of the $(M-OH)^+$ ion after dehydroxylation processes is a characteristic fragmentation pathway of hydroxyanthraquinones. For different hydroxyanthraquinones, hydrogen bond affects the intensities of the $(M-OH)^+$ peaks greatly. Thus, it is easy for us to distinguish 1-hydroxyanthraquinone from 2-hydroxyanthraquinone because the relative abundance of $(M-OH)^+$ in the former is several times higher than that in the latter compound.[16]

With the aid of the B3LYP calculations, eight dehydroxylation pathways are proposed, as shown in Scheme 3. We find that direct loss of OH group from benzene ring after C−O bond fission is dominant, and no transition states are obtained with our attempts. For example, owing to the symmetric structure, the lowest-energy isomer **1** will only break C1−O (or C8−O) bond to give the product **24** with the dissociation energy of 5.05 eV. For the cations **2** and **3**, cleavage of C1−O or C8−O bond will also produce the same product **24** with the dissociation energies of 4.98 and 4.82 eV, respectively. This is due to the mobility of hydrogen in molecular skeleton. Loss of OH from the cation **5** yields the product **25** with the dissociation energy of 4.35 eV. Interconversion between the fragments **24** and **25** could occur via OH group rotation about the C−O bond; the barrier is determined to be 0.5 eV from **24** to **25**. The energy for the loss of OH on C1 position from the cation **4** is a little larger and is calculated to be 5.82 eV. The product ion **26** from this step then undergoes hydrogen migration from O atom to C1 atom to form a more stable structure **27** via **TS39**. The barrier is determined to be 0.37 eV.

C9−O bond cleavage is another dominant fragmentation pathway to form $(M-OH)^+$ ion. DFT calculations reveal that cations **3** and **4** require the dissociation energies of 5.75 and 5.4 eV to break C9−O bonds and form the fragment **28**. Dissociation energy of 6.01 eV is needed for the cation **2** to produce the fragment **29**. This fragment then undergoes a hydrogen transfer from OH group to C9 atom and form the product **30**. The B3LYP barrier for this step is calculated to be 0.43 eV.

Among five conformers of $(M-OH)^+$, the product **24** along with OH group can be formed with the least energy, where the relative energy is calculated to be 13.29 eV. This energy is taken as AE value, which is in fairly good agreement with our experimental AE result (13.1 ± 0.1 eV).

4. Conclusion

The photoionization and dissociative photoionization of 1,8-DHAQ have been investigated by using IR laser desorption/tunable synchrotron VUV photoionization mass spectrometry. On the basis of experimental and theoretical results, the primary fragmentation pathways of 1,8-DHAQ are proposed to be consecutive losses of two CO groups and the loss of one OH group. The IE of 1,8-DHAQ and AEs for three major fragments of $(M-CO)^+$, $(M-C_2O_2)^+$, and $(M-OH)^+$ have been measured to be 8.54 ± 0.05, 10.8, 11.0, and 13.1 ± 0.1 eV by measurements of PIE spectra. These values are in fair-to-good agreement with the B3LYP calculations.

On the basis of theoretical calculations, five lowest-energy isomers of 1,8-DHAQ cation have been found to coexist via bond rotation or intramolecular PT. Consecutive losses of two carbon monoxides could occur from these isomers via undergoing a series of transition states and intermediates. Direct C−O bond cleavage is favored in the dehydroxylation process without any transition states.

Acknowledgment. This work has been supported by grants from the Chinese Academy of Sciences (YZ200764), the Specialized Research Fund for the Doctoral Program of Higher Education, the Natural Science Foundation of China (10705026), National Basic Research Program of China (973) under Grant no. 2007CB815204 and the China Postdoctoral Science Foundation (20070410793 and 20070420726).

Supporting Information Available: Structures of isomers, transition states, and intermediates. This material is available free of charge via the Internet at http://pubs.acs.org.

References and Notes

(1) Ohkuma, Y.; Hiraku, Y.; Kawanishi, S. *Free Radical Res.* **2001**, *34*, 595.
(2) Falk, H. *Angew. Chem.* **1999**, *111*, 3306.
(3) Müller, C.; Schroeder, J.; Troe, J. *J. Phys. Chem. B* **2006**, *110*, 19820.
(4) Kwon, Y. S.; Koh, J. Y.; Song, D. K.; Kim, H. C.; Kwon, M. S.; Choi, Y. S.; Wie, M. B. *Biol. Pharm. Bull.* **2004**, *27*, 723.
(5) Ferreiro, M. L.; Rodríguez-Otero, J. *J. Mol. Struct. (Theochem)* **2001**, *542*, 63.
(6) Arzhantsev, S. Y.; Takeuchi, S.; Tahara, T. *Chem. Phys. Lett.* **2000**, *330*, 83.
(7) Smulevich, G. *J. Chem. Phys.* **1985**, *82*, 14.
(8) Smulevich, G.; Foggi, P.; Feis, A.; Marzocchi, M. P. *J. Chem. Phys.* **1987**, *87*, 5664.

(9) Neuwahl, F. V. R.; Bussotti, L.; Righini, R.; Buntinx, G. *Phys. Chem. Chem. Phys.* **2001**, *3*, 1277.

(10) Pan, Y.; Gao, Y. H.; Yan, L.; Pan, H.; Chen, J. F.; Yu, S. Q. *Spectrochimi. Acta Part A: Mol. Biomol. Spectrom.* **2007**, *66*, 63.

(11) Waring, M. J. *Annu. Rev. Biochem.* **1981**, *50*, 159.

(12) Eriksson, M.; Norden, B.; Eriksson, S. *Biochemistry* **1988**, *27*, 8144.

(13) Nonaka, Y.; Tsuboi, M.; Nakamoto, K. *J. Raman Spectrosc.* **1990**, *21*, 133.

(14) Smulevich, G.; foggi, P.; Feis, A.; Marzocchi, M. P. *J. Chem. Phys.* **1987**, *87*, 5664.

(15) Gillispie, G. D.; Balakrishnan, N.; Vangsness, M. *Chem. Phys.* **1989**, *136*, 259.

(16) Beynon, J. H.; Williams, A. E. *Appl. Spectrosc.* **1960**, *14*, 156.

(17) Proctor, C. J.; Kralj, B.; Larka, E. A.; Porter, C. J.; Maquestiau, A.; Beynon, J. H. *Org. Mass Spectrom.* **1981**, *16*, 312.

(18) Pan, Y.; Zhang, T. C.; Guo, H. J.; Hong, X.; Qi, F. *J. Mass Spectrom.* **2008**, DOI: 10.1002/jms.1465, in press.

(19) Pan, Y.; Zhang, T. C.; Hong, X.; Zhang, Y. W.; Sheng, L. S.; Qi, F. *Rapid Commun. Mass Spectrom.* **2008**, *22*, 1619.

(20) Pan, Y.; Yin, H.; Zhang, T. C.; Guo, H. J.; Sheng, L. S.; Qi, F. *Rapid Commun. Mass Spectrom.* **2008**, *22*, 2515.

(21) Huang, C. Q.; Yang, B.; Yang, R.; Wang, J.; Wei, L. X.; Shan, X. B.; Sheng, L. S.; Zhang, Y. W.; Qi, F. *Rev. Sci. Instrum.* **2005**, *76*, 126108.

(22) Qi, F.; Yang, R.; Yang, B.; Huang, C. Q.; Wei, L. X.; Wang, J.; Sheng, L. S.; Zhang, Y. W. *Rev. Sci. Instrum.* **2006**, *77*, 084101.

(23) Frisch, M. J.; Trucks, G. W.; Schlegel, H. B.; Scuseria, G. E.; Robb, M. A.; Cheeseman, J. R.; Montgomery, J. A., Jr.; Vreven, T.; Kudin, K. N.; Burant, J. C.; Millam, J. M.; Iyengar, S. S.; Tomasi, J.; Barone, V.; Mennucci, B.; Cossi, M.; Scalmani, G.; Rega, N.; Petersson, G. A.; Nakatsuji, H.; Hada, M.; Ehara, M.; Toyota, K.; Fukuda, R.; Hasegawa, J.; Ishida, M.; Nakajima, T.; Honda, Y.; Kitao, O.; Nakai, H.; Klene, M.; Li, X.; Knox, J. E.; Hratchian, H. P.; Cross, J. B.; Bakken, V.; Adamo, C.; Jaramillo, J.; Gomperts, R.; Stratmann, R. E.; Yazyev, O.; Austin, A. J.; Cammi, R.; Pomelli, C.; Ochterski, J. W.; Ayala, P. Y.; Morokuma, K.; Voth, G. A.; Salvador, P.; Dannenberg, J. J.; Zakrzewski, V. G.; Dapprich, S.; Daniels, A. D.; Strain, M. C.; Farkas, O.; Malick, D. K.; Rabuck, A. D.; Raghavachari, K.; Foresman, J. B.; Ortiz, J. V.; Cui, Q.; Baboul, A. G.; Clifford, S.; Cioslowski, J.; Stefanov, B. B.; Liu, G.; Liashenko, A.; Piskorz, P.; Komaromi, I.; Martin, R. L.; Fox, D. J.; Keith, T.; Al-Laham, M. A.; Peng, C. Y.; Nanayakkara, A.; Challacombe, M.; Gill, P. M. W.; Johnson, B.; Chen, W.; Wong, M. W.; Gonzalez, C.; Pople, J. A. *Gaussian 03* Gaussian, Inc.: Wallingford, CT, 2004.

(24) Ortiz, J. V. *J. Chem. Phys.* **1996**, *104*, 7599.

(25) Dolgounitcheva, O.; Zakrzewski, V. G.; Ortiz, J. V. *Int. J. Quantum Chem.* **2000**, *80*, 831.

(26) Dolgounitcheva, O.; Zakrzewski, V. G.; Ortiz, J. V. *J. Am. Chem. Soc.* **2000**, *122*, 12304.

(27) Linstrom, P. J.; Mallard, W. J *NIST Chemistry Webbook* National Institute of Standard and Technology: Gaithersburg, MD, 2005; Number 69, http://webbook.nist.gov.

(28) Monks, P. S.; Stief, L. J.; Tardy, D. C.; Zhang, Z. Y.; Kuo, S. C.; Klemm, R. B. *J. Phys. Chem.* **1995**, *99*, 16566.

(29) Tsunoyama, H.; Misaizu, F.; Ohno, K. *J. Phys. Chem. A* **2004**, *108*, 5944.

(30) Cheng, B. M.; Chew, E. P.; Liu, C. P.; Yu, J. S. K.; Yu, C. H. *J. Chem. Phys.* **1999**, *111*, 10093.

(31) Dryza, V.; Addicoat, M. A.; Gascooke, J. R.; Buntine, M. A.; Metha, G. F. *J. Phys. Chem. A* **2005**, *109*, 11180.

JP806171H